Sensing of the Molecular Spin in Spin-Crossover Nanoparticles with Micromechanical Resonators

Dugay, Julien; Giménez-Marqués, Mónica; Venstra, Warner J.; Torres-Cavanillas, Ramón; Sheombarsing, Umit N.; Manca, Nicola; Coronado, Eugenio; van der Zant, Herre

Important note
To cite this publication, please use the final published version (if applicable).
Please check the document version above.

SENSING OF THE MOLECULAR SPIN IN SPIN CROSSOVER NANOPARTICLES WITH MICROMECHANICAL RESONATORS

Dugay Julien,*,† Mónica Giménez-Marqués,‡ Warner J. Venstra,† Ramón Torres-Cavanillas,‡ Umit N. Sheombarsing,† Nicola Manca,†,¶ Eugenio Coronado,*,‡ and Herre S.J. van der Zant†

†*Kavli Institute of Nanoscience, Delft University of Technology, Lorentzweg 1, 2628 CJ Delft, The Netherlands*

‡*Instituto de Ciencia Molecular (ICMol), Universidad de Valencia, c/Catedrático José Beltrán, 2, 46980 Paterna, Spain*

¶*Physics Department, University of Genoa, Via Dodecaneso 33, 16146 Genova, Italy*

E-mail: julien.dugay@gmail.com; eugenio.coronado@uv.es

Abstract

In the past years, the use of highly sensitive Silicon Micro-Electro-Mechanical cantilevers has been proposed as a tool to characterize the spin-crossover phenomenon by employing fast optical read-out of the motion. In the present work, Fe^{II}-based spin-crossover nanoparticles of the well-knownv[Fe(Htrz)^2(trz)](BF$_4$) complex wrapped with a thin silica shell of different sizes will be studied by means of silicon micro-resonators. The silica shell will enhance its chemical stability, while the low thickness allows a proper mechanical coupling between the cantilever and the spin-crossover core. To maximize the sensing of the spin-crossover phenomena different cantilever geometries

1

and flexural modes were employed. In addition, the experimental observation was also compared by COMSOL numerical simulations, which are in close agreement with them. The probe of spin-crossover phenomena with micro and nanoelectro mechanical actuators offers the possibility to prepare smart sensing memory devices near/above room temperature.

Introduction

Micro- and nanomechanical systems can be treated largely within the framework of bulk elasticity theory. This field has been in development for over half a century[1] with growing interest driven by the tremendous amount of potential day-life applications.[2] The development of the atomic force microscope in the mid-80's has sparked the advent of micro-nano cantilever-based platforms for physical, chemical and biological sensing.[3–5] Operation of micro- and nanoelectromechanical sensors (MEMS/NEMS) involve measurements of static deflections, dynamical resonant frequency or damping characteristics of the resonators. Their mechanical responses are caused by a gradient of mechanical stress that can be generated i\ by changes in temperature (in particular for cantilevers made of two layered materials with different thermal expansion coefficients),[6] ii\ molecular adsorption and interfacial chemical reactions[7] or iii\ materials showing solid-state phase transition with an associated lattice expansion up to 1%.[6,8,9]

The high-stress sensitivity of MEMS/NEMS for elaborating smart molecular actuators has been proposed only recently,[10–13] with one example reported in 2016 for Silicon MEMS cantilevers covered by thermally-evaporated spin-crossover (SCO) thin films.[14] In particular, SCO materials are interesting systems in this respect as they show a substantial change in molecular volume and shape while adapting to environmental perturbations (*c.g.*, up to 13 %).[15] This change results from an entropy-driven switching from a low-spin state (S=0, volume reduced) to a high-spin state (S=2, expanded volume)[16] that can be translated into mechanical work.[17] Moreover, their physico-chemical properties (electronic, optical, mechanic,

magnetic) can be adjusted and tuned to specific target applications by external stimuli such as temperature and pressure variations, light irradiation, magnetic field[18] and electric field[19] or chemical species.[20] Further, these materials enable low-cost efficient production and self-assembly techniques on various substrates.[21,22]

Two key works demonstrated the realization of micromechanical resonators controlled by temperature. Urdampilleta and coauthors employed an organic MEM device made of a polyethylene naphtalate substrate covered with poly(vinylidene fluoride-trifluoroethylene, sandwiched between two thin layers of aluminum.[23] Such a device is associated with a low Young's modulus and a high aspect ratio, demonstrating large resonance frequency shifts (sometimes accompanied with hysteresis loops), dominated by the total surface stress, which is consistent with our work. Besides, M. Manrique-Juárez et al. demonstrated an upward bending of the cantilever upon the low-spin to high-spin transition in agreement with the change in the lattice parameters of their complex (corresponding to a compressive strain of about -1% estimated along the cantilever length).[14] Besides, they reported a decrease of approximately 66 Hz in the resonance frequency as well as by the drop for the quality factor around the spin transition. In both cases, the memory effects in SCO films (with thicknesses ranging between 0.14 and 4 μm) were observed well below room temperature.

In this work, we exploit sensitive Si MEMS cantilevers to study a set of hybrid core-shell SCO nanoparticles (NPs) by employing fast optical read-out of the motion of microcantilevers. We coated these micro-resonators with thin-films of hybrid SCO@SiO$_2$ NPs by drop-casting method. The NPs were made from the reference one-dimensional (1D) Fe^{II}-based SCO complex of formula [Fe(Htrz)$_2$(trz)](BF$_4$) offering notably wide hysteresis in their physical properties' transitions even above room temperature.[24–26] These SCO NP cores, tunable in size, were wrapped with particularly thin silica (SiO$_2$) shell to provide enhanced chemical stability while allowing mechanical coupling with the cantilevers.[27] We investigated four different cantilever geometries and their respective three lowest resonant frequency flexural modes for SCO detection. While the cores of the SCO NPs switch from

the low-spin to the high-spin state, a systematic and reversible increase in the cantilever resonance frequency was observed. Concomitantly, a drop of the quality factor and of the static bending of the cantilever was revealed. The experimental observations are corroborated by a finite element analysis, which quantitatively reproduces the temperature dependence of the resonant frequencies and static deflections of the hybrid SCO@SiO$_2$ NPs.

Methods

Synthesis of hybrid [Fe(HTrz)$_2$(Trz)](BF$_4$)]@SiO$_2$ NPs

For the synthesis of hybrid SCO NPs **1** and **2** we followed a modified protocol of the reverse-micelle synthesis[27] developed by Herrera and Colacio and co-workers. Parameters such as the concentration of SCO precursors Fe(BF$_4$)$_2$. 6H$_2$O and 1,2,4-1H-Triazole) and the addition of the SiO_2 precursor to the organic phase, were selectively modified to respectively tune both, the size of the SCO core and the thickness of the inorganic shell. In a general procedure, two microemulsions containing aqueous solutions of the precursors $Fe(BF_4)_2.6H_2O$ (0.5 mL, 1.25 M in case of NPs 1 and 1.5 M in case of NPs 2) and the ligand 1,2,4-1H-Triazole (0.5 mL, 3.75 M for 1 and 4.5 M in 2) were prepared by mixing with an organic solution of Triton X.100 (1.8 mL, ω = 9 for 1 and 2.2 mL, ω= 5 in 2), n-hexanol (1.8 mL), TEOS (0.1 mL) and cyclohexane (7.5 mL). The microemulsions were mixed and left to react for 24 h in 1 whereas were only stirred for 2h in 2. NPs were collected after precipitation by adding acetone to destabilize the microemulsion, followed by 4 washing cycles with ethanol to remove the excess of surfactant, and one with acetone. Finally, the powdered samples were dried at 70 ºC for 2 h.

Deposition of NPs on microcantilevers

Tipless silicon cantilevers (All-In-One, Budget Sensors) were used with four distinct geometries listed in the Supplementary Table S2. The cantilevers were decorated with silica (SiO$_2$)

coated NPs using the drop-casting method (the deposition is performed only on one side of the cantilever). This deposition technique is well-suited for the present NP systems, since the SCO active cores are stabilized by a polar SiO_2 shell. To obtain sufficient coverage, we adjusted the colloidal solution concentration by the following two steps. First, 5 mg of dry $SCO@SiO_2$ NP powder was suspended in 2 ml of ethanol and stirred in an ultrasonic bath for 15 minutes. Ethanol has a low boiling point and is polar, and readily disperses the $SCO@SiO_2$ NPs. A concentration of 2.5 mg/ml showed a good stability over time with no signs of precipitation. In the second step, the suspension was diluted 100 times in ethanol and dropcasted onto the chip using a micropipette. Excess liquid was removed with absorbing paper, and most of the remaining solvent evaporated during thermal cycling in the vacuum, as is discussed in the main text.

Deposition of ethanol on microcantilevers.

A similar device was prepared for acting as a reference for the study by dropcasting ethanol onto the chip. Excess liquid was removed with absorbing paper, and most of the remaining solvent evaporated during thermal cycling in the vacuum, as is discussed in the main text.

Measurement of the temperature-dependent mechanical response

Measurement of the mechanical response. An optical lever is used to detect the static and dynamic displacements of the cantilevers. The cantilevers are placed in a small vacuum chamber to reduce viscous air friction and potential contamination of the SCO NP layer. The cantilevers are mounted on a manual positioning stage, which enables the selection of the cantilever of interest. The resonance modes are excited by supplying the alternating voltage from a network analyzer (Agilent 4395A) to a piezo actuator (Piezo Systems Inc.) placed in the vicinity of the cantilever chip. The signal from the PSD was detected by the network analyzer and recorded on a computer. The measurements are conducted at a pressure of 2×10^{-6} mbar while the excitation voltages are low enough to ensure that the

cantilever vibrates in the linear regime. The static bending of the cantilever is detected by measuring the dc-component of the PSD voltage using a multimeter (Keithley DMM199). The incident probe laser power is well below 1 mW, as to eliminate effects of laser heating.

Temperature control details. The temperature of the chip is determined by measuring the resistance of an NTC placed close to the chip on the Peltier element. A PID controller is implemented in LabView and a custom-built power amplifier was employed to drive the Peltier element towards the temperature setpoint. To remain in the quasi-static measurement regime, all temperature sweeps are performed at 1 °C.min^{-1} and the temperature variation during a frequency response measurement was below 0.1 °C over a range of 15 - 135 °C. This range covers the temperatures at which the hysteretic SCO was expected.
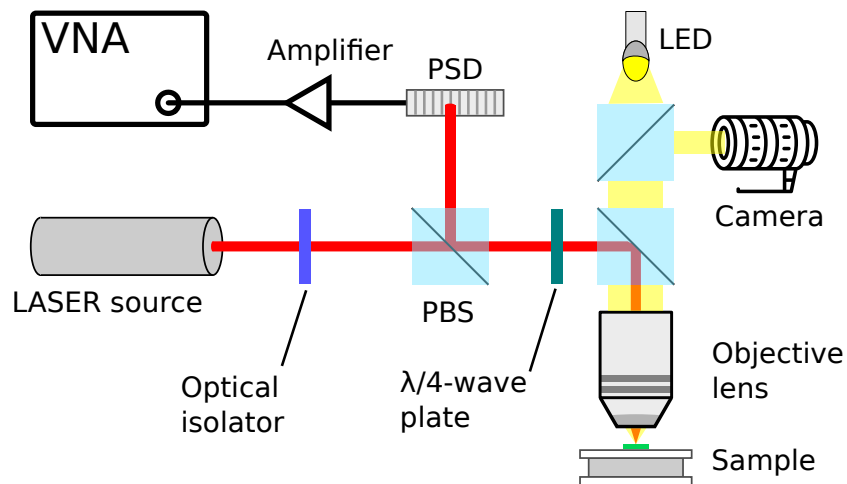
Figure 1: Schematic of the optical lever system. PBS: Polarizing Beam Splitter; PSD: Position Sensitive Device; LED: Light Emitting Diode.

The Figure 1 describes the optical lever system. The output of a temperature-stabilized laser diode, emitting at 658 nm, enters through a polarizer and passes through a polarizing beam splitter (PBS) and a quarter wave plate. The beam is directed onto the cantilever of interest, which can be selected by adjusting position of the vacuum chamber containing the cantilevers with a micropositioning stage, while monitoring the cantilever position using the camera. The reflection of the cantilever surface passes again through the $\lambda/4$ plate and is

deflected by the PBS onto the Position Sensitive Device (PSD). To detect the mechanical response, the cantilevers are excited by supplying the output of a Vector Network Analyzer (VNA) to a piezo-actuator placed near the samle in the vacuum chamber. The magnitude- and phase response of cantilever to the excitation signal is detected by the network analyzer and recorded on a computer (see Methods for more experimental details).

Errors in measurements. Besides, the error results on our data is comparable with the marker size. Indeed, the error on the frequency measurements can be evaluated considering the spectrum sampling density of the vectorn network analyzer, which was selected at measurement time and corresponded to 10 Hz. the temperature is not calibrated so the error is evaluated considering the temperature fluctuations (noise) of the temperature sensor, which are below 50 mK. The error on the COMSOL simulations is not statistical and is given by the selected convergence criterion, well below 10^{-3}. All of these values are not visible in the reported plots and thus not included.
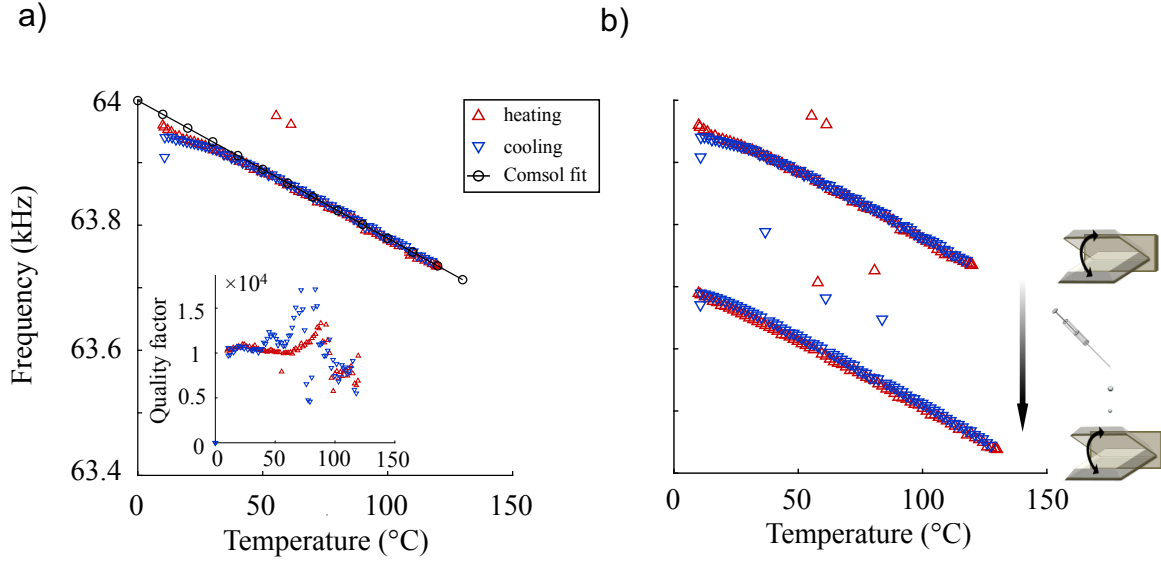
Results and Discussion

Figure 2: (a) Resonance frequency of the bare cantilever (*chip A, cantilever B*, fundamental mode) across the temperature range of interest. The experiment shows one cycle of controlled heating (red triangles pointing upwards) followed by controlled cooling (blue triangles pointing downwards). The black solid line represents a finite element model (see main text). Over the temperature range 15–135 °C the resonance frequency varies by 0.5 %. The associated quality factor is presented in the inset. (b) Adding the solvent (ethanol) causes the overall response shifting to a lower frequency. After pre-conditioning the cantilever by 15 thermal cycles, the response stabilizes at a residual frequency shift of -260 Hz.

Before depositing the SCO NPs, the temperature dependence of the mechanical properties of the bare cantilevers was characterized. Figure 2.a shows the resonance frequencies of the fundamental mode (*chip A, cantilever B*), obtained by fitting a harmonic oscillator to the detected frequency responses. The resonance frequency decreases in proportion with the temperature (-2 Hz / °C), which is expected from the temperature-dependence of the elastic modulus of silicon in this temperature range.[8] The quality factors being almost temperature independent, see inset, indicated that the silicon cantilevers vibrate in the intrinsic damping regime,[28] *i.e.*, the major damping processes occurs in the cantilever, while the medium has a negligible effect. Comparable responses were obtained for higher flexural resonance modes and for the other cantilevers on the same chip (see Supplementary Figures S4 and S5). A finite element model of the coupled thermal-mechanical problem captures the temperature dependence of the resonance frequency, as is shown by the black

thin line in Figure 2.a, and is also in good agreement with the other cantilever geometries (see Supplementary Figures S4 and S5).

We selected NPs based on the renowned $[Fe(Htrz)_2(trz)](BF_4)$ (Htrz = 1,2,4-triazole and trz = 1,2,4-triazolate) SCO material. It was already established that a shell of SiO_2 grown around the NP confers robustness and allows functionality.[29,30] For the application in the MEMS sensors, it is important that the interaction of the NPs with the cantilever is maximized. For this reason, we obtained a set of hybrid SiO_2-SCO NPs presenting different sizes surrounded with a very thin inorganic shell of only a few nm, enough to protect and preserve the SCO core while allowing for sufficient interaction with native oxide of the Si cantilever (see Methods for experimental details of the synthesis). The NPs **1** and **2** in this study exhibit different sizes (prismatic shape with dimensions 87×54 nm and cubic shape with dimension 28 nm covered with a SiO_2 shell of 1 nm and 0.5 nm, respectively) as confirmed by TEM characterization (Supplementary Figure 1). Deposition proceeded by first suspending the SCO NPs in pure ethanol and drop-casted them on top of the cantilevers (see Methods for details on NP deposition), additionally as a reference, a device covered with pure ethanol following the same method was carried out. SEM inspection of for example *chip A*, carried out after drop-casting and numerous mechanical measurements as a function of temperature, demonstrated the presence of non-coalesced SCO NPs onto the chip but also on all the cantilevers (see Figure S1.b and the Supplementary Figure S7).

The discussion below will focus primarily on NPs **1**. Some results on NPs **2** will be reported for comparison at the end of the section. Drop-casting a suspension of SCO NPs on a cantilever introduces frequency shifts due to the added mass of the NPs and of the solvent. To distinguish these effects from signals that are associated with the intrinsic behaviour of the SCO NPs, we first examined the effect of depositing the solvent. A significant drop of the resonance frequency was observed after the deposition, which diminished as the solvent evaporated while cycling the temperature and then stabilized at -260 Hz after 15 temperature cycles. Figure 2.b shows the stabilized (after 15 cycles) temperature dependence of the reso-

9

nance frequency (lower curve) in comparison to the bare cantilever (upper curve). The downward shift was attributed to remaining adsorbed solvent molecules, which total mass Δm can be calculated from the frequency shift Δf as $\Delta m = -2\Delta f/f_0 \times m_0$, where $m_0 = 23.1$ ng is the mass of the cantilever and $f_0 = 63.93$ kHz is the resonance frequency of the bare cantilever.[31] The mass of remaining adsorbed solvent molecules was estimated to of about 0.19 ng.
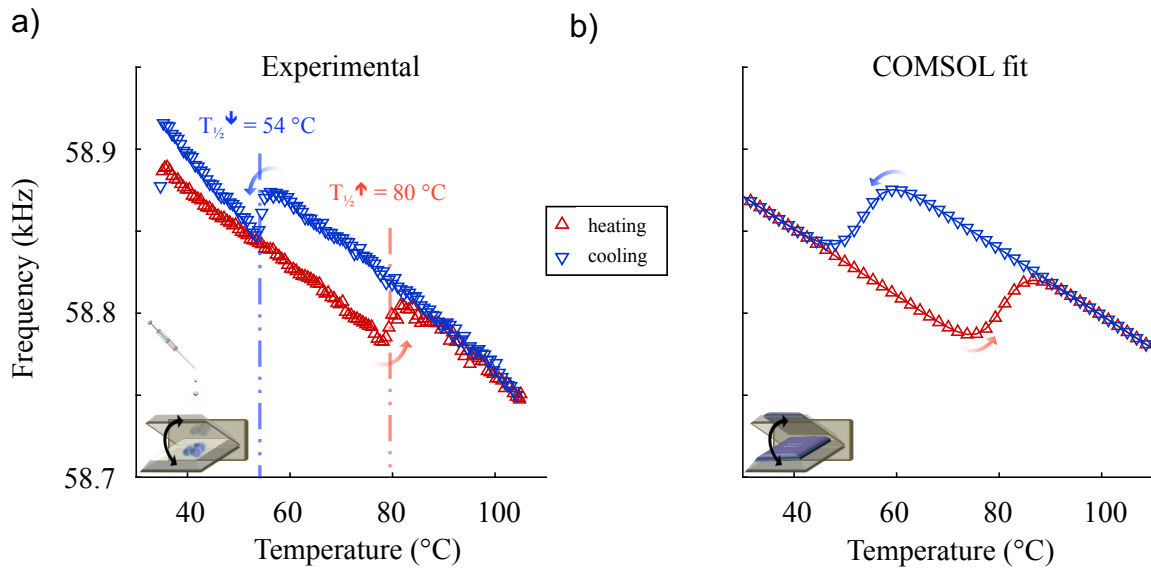

Figure 3: Comparison of experimental (a) and simulated (b) thermal hysteresis loops detected in the fundamental resonance frequency of hybrid resonators. On the left, hybrid SCO NPs (sample **1**, see Supplementary Information) are covering the cantilever type (same sample as in Fig 2). The data presented correspond to the 7th thermal cycle reproducibly observed after a pre-conditioning (consisting of 15 thermal cycles); the change in frequency corresponds to the mass addition of 3.44 ng. Simulations were carried out by approximating this mass to a homogeneously distributed thin layer covering the cantilever where the latter is endowed by the same spin-dependent physical properties as the SCO NPs **1** (see Table S4 in Supplementary Information). A good agreement between experimental and numerical results is obtained when the thickness of the thin layer is set to 650 nm.

Figure 3 displays the fundamental resonance frequency recorded after nanoparticle deposition and after thermal preconditioning (6 times reproduced thermal hysteresis loops; same sample as the one used in Fig. 2).

Considering the resonant frequency shift observed after depositing the NPs by drop-casting, we evaluate that the mass of the added NPs is equal to 3.44 ng corresponding to

a frequency shift of 4.8 KHz. This frequency shift corresponds to the subtraction of the resonant frequency before and after drop-casting of the colloidal solution of SCO NPs and after stabilization in similar conditions and using the same cantilever (see figures 1.b and Figure 2.a). This mass corresponds to a NP volume of about 1.9×10^{-6} mm^3 in the low-spin state). Note that the slight shift observed after solvent drop-casting was beforehand subtracted from the total resonance frequency shift. Assuming that the top face and both undercut sides of the cantilever are uniformly covered by the NPs and that their lengths are aligned within the monolayers, we estimated that the thickness of the resulting thin film falls in a range of 330-360 nm (corresponding to about 6 monolayers (MLs), see calculation details in Supplementary Information). This estimation seems plausible in view of the SEM observations reporting the presence of NP islands sometimes thicker than *ca.* 6 MLs (see Figure S1.b and Figure S7 in Supplementary Information).

In Figure 3a, a slight decrease of the resonance frequency with increasing temperature of about 0.34 % over 70 °C (*i.e.*, of about -2.5 Hz /°C) was observed. This value is very close to the linear contribution revealed earlier from the reference cantilever (of about -2 Hz /°C, see Figure 2). More remarkable than the background contribution was the appearance of a well-pronounced and reproducible hysteresis loop in the temperature dependence of the resonance frequency. The transition temperature onset above room temperature is in agreement with the magnetic measurements obtained on powder samples (see Figure S3 and Table S1 in Supplementary Information) and transport measurements using graphene nanogaps.[32] We emphasize that control experiments revealed that hysteresis loops in the resonance frequency were neither observed for the same cantilever as-received nor after deposition of drops of pure ethanol (see Figure 2). We thus rationalize that the bistable mechanical response accompanied by wide hysteresis loops correspond to the spin-state dependent physical properties of investigated hybrid SCO@SiO$_2$ NPs.

Another important observation in Figure 3 is the abrupt increase of the resonance frequency when the SCO NPs undergo the $LS \rightarrow HS$ transition (and vice versa while decreasing

temperature). This corresponds to a frequency change of about 30 Hz for the *cantilever B* of the chip A (or 4.3×10^{-2} %). This behaviour seems at a first glance in contradiction with a recently published work reporting a slight opposite downshift of -0.5 Hz (or 1.18×10^{-2} %) detected using thicker microcantilevers.[14] We attribute the observed upshift upon low-spin to high-spin thermal transition to the predominant role of the surface stress when thin structures are probed. In particular, the substantial volume increase of the SCO@SiO$_2$ NPs in the high spin-state leads to a larger curvature and therefore effective rigidity of the cantilever. This in turn causes the increase observed in the resonant frequency. As only one simplified analytical model has been developed to account for this phenomenon,[14] we calculated the resonance frequencies of the hybrid resonators with a finite element-based numerical model.

Indeed, the temperature-dependence of the resonance frequencies of the composite SCO@SiO$_2$ NPs / cantilever was calculated numerically using the structural mechanics module of COMSOL Multiphysics 5.2. The cantilever geometry was parametrized in MATLAB and transferred via LiveLink MATLAB to COMSOL. Both the static bending and the dynamic response (multiple flexural modes) were calculated for the four cantilevers, coated with SCO NP's films having a variable thickness. The three-dimensional models closely resemble the genuine cantilever geometry. For convenience the "picket"-shaped end of the cantilever was simplified to a rectangular shape. The material properties used for the model are listed in Supplementary Table S2.

This numerical model allows us to simulate genuine stress softening, geometric changes and temperature dependence of a MEMS device covered by a SCO thin-film of tunable thickness, which were determined by accurate analysis using numerical simulations (see methods for details). In the calculations, we assume a homogeneously distributed thin NP layer with a thickness corresponding to the one estimated from the resonant peak shifts. The physical properties used for the SCO@SiO$_2$ NPs are summarized in Supplementary Table S4). The thin-film thickness is varied from about one hybrid NP monolayer (ML) up to about 5 μm. The resulting numerical simulations substantiate the experimental upshifts of the resonance

12

frequency observed upon $LS \rightarrow HS$ transition as displayed in Figure 3.b (see the Supplementary Figure S13). The anti-clockwise loop direction observed experimentally is consistent with our numerical results that also predict an anti-clockwise loop direction for SCO films with thicknesses below 3.6 and $1.8\mu m$ respectively for samples 1 and 2. For thicker films an inversion of the hysteresis loop direction from anti-clockwise to clockwise is expected. The simulated resonance frequency shift and the relative change in resonance frequency as a function of temperature are in very good agreement with experimental results if the NP layer thickness is set to 650 nm. This value is within a factor of two compared to the one experimentally estimated from the change in frequency.

Numerous parameters can affect the cantilever resonance frequencies such as, $i|$ fabrication related factors (geometry of cantilevers, thickness nonuniformity) $ii\backslash$ the surface state at the interface between the cantilever and the covering material, $iii|$ the change of mechanical properties of the covering material (Young's modulus, mass density, thermal dilatation) and $iv|$ extrinsic factors (adsorbed masses, ambient pressure and temperature).[31] When fabricated and measured in similar conditions, it is expected that changes in surface stresses govern the resonance frequency shift for thin structures when $b(width)/h(thickness) >> 1$, while a change in geometry due to elastic deformation or a volume change of a covering layer will prevail for thicker devices.[33]
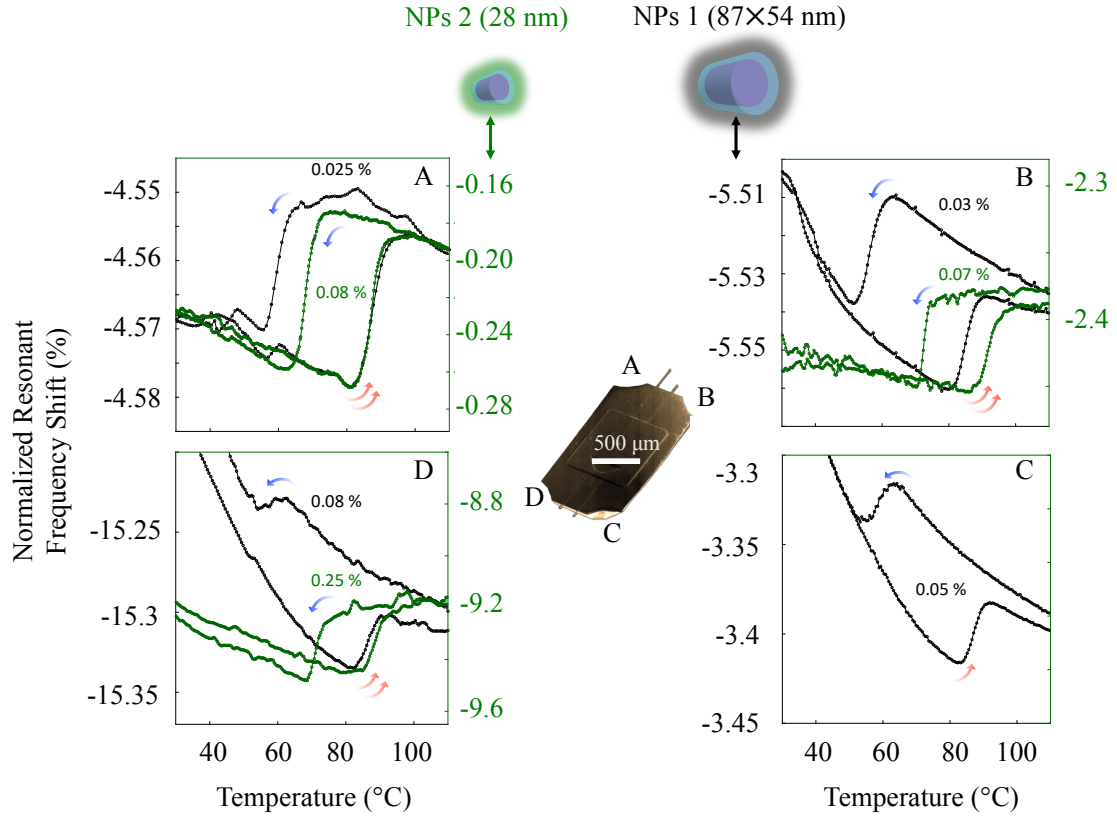
Figure 4: Normalized resonant frequency shift of SCO@SiO$_2$/Si microcantilevers as a function of temperature for the four cantilever geometries (Chip B and C). The shift and normalization is with respect to the first flexural resonant frequency of the bare cantilevers. These data were acquired after thermal pre-conditioning (of about 15 thermal cycles) and reproduced multiple times. The wide thermal hysteresis loops in the mechanical responses near room temperature correlate with the SCO@SiO$_2$/Si NP morphologies. This behaviour has been consistently observed for the first, second and fifth flexural vibrational eigenmode.

To shed more light on the mechanism behind the frequency changes and hysteresis, similar experiments have been performed with smaller NPs (sample 2) and with cantilevers with different b/h ratios. In Figure 4 we present the lowest flexural resonant frequency shifts as a function of temperature for both NPs, **1** and **2**. The temperature-dependent elastic modulus of the bare cantilevers are eliminated by subtracting the resonant frequency at a given cantilever geometry before NP deposition with that observed after NP deposition and normalized to the bare cantilever values, in each case at the same temperature. Remarkably, for both NP morphologies, clear thermal hysteresis loops are observed for each of the four

14

cantilever geometries (see Supplementary Table S2 for cantilever dimensions). Similar anti-clockwise and wide thermal hysteresis loops are consistently seen, not only for the lowest flexural eigenmode but also for the second and fifth ones (for the longest cantilevers, see for instance Supplementary Figure S11). Note that the normalized shift in the resonance frequency upon spin-transitions follows the cantilever resonance frequency, which increases when the cantilever length is reduced (from 0.025 % to 0.08 % and 0.08 % to 0.25 % for **1** and **2** respectively as displayed in Figure 4).

The frequency shift arises from the mechanical expansion of SCO NPs upon spin-transition and the consequent mechanical stress applied to the cantilever surface. The frequency shift is a result of the dynamical interaction between localized stress and structural deformation, i.e. it matters if the SCO NPs are located in a node of the eigenfunction of a particular mode or not. Changing the modes and length makes the nodes to be located in different positions and thus results in different frequency shift. When comparing the numerical and experimental results we conclude that smaller cantilevers exhibit the best sensitivity in terms of detection in the change of surface stress and accompanying shift in the mechanical eigen frequencies upon the SCO transition, which is in good agreement with our experimental observations (see Supplementary Information Figure S13). Moreover, a better sensitivity is expected for higher flexural modes, which is also observable in our measurements (see the Supplementary Figures S14 and S12 respectively for numerical simulation and experimental results). The amount of the frequency increase is determined by the balance between the total rigidity of the structure and the accumulated stress.[33] The structural rigidity is determined by the geometry of the cantilevers; a higher sensitivity is expected for cantilevers with a larger surface/volume ratio. The accumulated stress is enhanced for the highest vibrational modes and modified by the change in volume of the NPs upon the SCO transition.

To investigate the SCO temperatures in more detail, we collected the detected transition temperatures -which turned out to be independent of cantilever geometry and vibration mode - and plotted them in a histogram. Figure S15 compiles the experimental set of 152

measured SCO transition temperatures in cooling ($T^{LS \leftarrow HS}$, blue) and heating ($T^{LS \rightarrow HS}$, red) modes. The transition temperatures have been extracted for NPs **1** (43 thermal cycles, black curve) and **2** (33 thermal cycles, green curve). Statistically a clear NP size effect on the transition temperatures is demonstrated where the expectation value of $T^{LS \rightarrow HS}$ is 57 °C for **1** while for **2** the transition occurs at T = 72 °C; for $T^{LS \leftarrow HS}$, the expectation values are 85 and 90 °C for **1** and **2**, respectively.

These transition temperatures can be compared with those of SQUID measurements as both approaches employ *quasi*-static measurements (see Methods). Interestingly, a slight shift towards lower temperatures and narrower width loops are observed when compared with SQUID measurements. Moreover, ($T^{LS \leftarrow HS}$ is size independent and ($T^{HS \rightarrow LS}$ is size dependent), while the opposite behaviour is observed for transition temperatures extracted from SQUID measurements. One cannot exclude that the differences in sample environmental pressure of the two types of experiments causes the slight mismatch in transition temperatures: SQUID magnetometry is performed under a few mbar partial He pressure, while the MEMS measurements resented in this paper were performed under a high vacuum of about 2.10^{-6} *mbar*. It is known that a decrease of the pressure reduces the transition temperatures of SCO compounds.[34,35] However, the downward shift is expected to be negligible for this pressure range and should occur in a symmetric way,[36] which is not the case. We thus speculate that the difference in SCO transition temperatures, when comparing powdered samples (SQUID measurements) and small assemblies of hybrid SCO NPs, may be due to a difference in interparticle elastic interactions (3D vs. 2D respectively) and/or to the mechanical coupling with the supporting silicon cantilever. Both contributions could modify the elastic surface stress resulting in a volume misfit change between the SCO core and the SiO_2 shell of the NPs. Indeed, the interplay between lattice vibrational and mechanical features of the core-shell NP as the prominent mechanism for memory effect features.[37,38] On the other hand, one cannot rule out that acoustic phonons emitted from the environment (not necessarily similar in a SQUID or in a MEMS setup), are more prone to efficiently

couple to the core-shell NPs phononic density of states spectrum rather than the optical ones.[39] However, a comprehensive theoretical study encompassing the elastic interactions between core-shell NPs in direct contact with a supporting substrate is not yet available in the literature. Such effect has thus to be more thoroughly investigated both theoretically and experimentally.

A change in the surface stress accumulation not only affects the resonance frequency, but also the static curvature of the cantilever. For this reason, we also detected the static deflection of the cantilevers by measuring the dc-component of the signal from the position sensitive device (see Figure S10.b in Supplementary Information).[40] A rather large background slope is introduced when heating the setup, which causes a rotation of the chip due to thermal expansion mismatch. On top, a clear hysteresis is observed in the cantilever curvature, which occurs at the same temperatures as in the dynamic measurements. The spin-state dependence of the signal cannot arise from the well-established spin-state dependence of the optical absorption of the triazole-based SCO compound[41] as these compounds absorb a little bit more (and thus reflect less) at the laser wavelength upon $LS \rightarrow HS$ crossover, while the opposite behaviour is observed (*e.g.* a more reflected signal). As a control experiment, a bare cantilever was measured in the same conditions, displaying solely the exponential decrease when increasing temperature (see Figure S10.a in Supplementary Information).

It is also of interest to investigate the damping characteristics of the cantilevers as a function of temperature. The damping figure of merit is embodied by the quality factor of the resonance, which represents the ratio between the total energy in the resonance mode and the energy that is dissipated per cycle. Remarkably, as it is shown in the Supplementary Figure S8.b, the Q-factor drops upon the $LS \rightarrow HS$ transition when increasing temperature, whereas the cantilever vibrates at a higher resonance frequency. In addition for the smallest SCO NPs **2**, we observe distinct minima in the Q- factor near the onset of the spin transition (see Supplementary Figure S9.b). Furthermore, for both SCO NP sizes and for all background resonance modes considered, we detect a systematic increase of the Q-factor

17

with increasing temperature. In contrast, a linear drop usually occurs for silicon beams as the temperature is raised due to thermoelastic damping at constant pressure. As far as the drop of the Q-factor on going from the LS to the HS state is concerned, this behaviour is not related to the SCO-induced internal stress (where Q would increase with the frequency) but suggests a significant increase of the damping force when the cores of the NPs are in the HS state. At this point, we can only speculate that this increase could emanate from the increased contact area (caused by the larger volume in the HS state) between the SCO@SiO$_2$ NPs and the cantilever, thereby enhancing the friction at the NP-cantilever interface.

While the MEMS devices here were introduced as a characterization tool, we note that the large volumetric changes of SCO materials present a significant potential for their use as actuator materials in MEMS and NEMS devices.[42] Compared to the piezoelectric actuators that are widely deployed in MEMS devices, the strain introduced by the SCO is higher (by 2-3 orders of magnitude), while the presence of hysteretic properties above room temperature enables new actuator-and-hold schemes. These properties could be harnessed, *e.g.,* by incorporating metallic heaters in the hybrid MEMS device.[43]

During the preparation of this manuscript we became aware of two related works in which thermo-active MEMS devices were actuated at their resonance frequency by a voltage or magnetic field while the mechanical vibration detection was performed by piezoresistors.[23,44] The first one employed an organic MEM device made of a polyethylene naphtalate substrate covered with poly(vinylidene fluoride-trifluoroethylene, sandwiched between two thin layers of aluminum. Such a device is associated with a low Young's modulus and a high aspect ratio, demonstrating large resonance frequency shifts (sometimes accompanied with hysteresis loops), dominated by the total surface stress, which is consistent with our work.[45] Second, in a very similar manner as we did, M.Manrique-Juárez *et al.* demonstrated an upward bending of the cantilever upon the $LS \rightarrow HS$ transition in agreement with the change in the lattice parameters of their complex (corresponding to a compressive strain of about -1% estimated along the cantilever length). Besides, they reported a decrease of approximately

66 Hz in the resonance frequency as well as by the drop for the quality factor around the spin transition.[44] In both cases, the memory effects in SCO films (with thicknesses ranging between 0.14 and 4 μm) were observed well below room temperature.

Conclusion

In this work, we have used microcantilevers to detect the thermally induced cooperative spin-state switching of hybrid SCO NPs above room temperature. We have employed fast optical read-out of the motion of tip-less silicon AFM cantilevers with various geometries ranging from $500 - 100 \pm 10$ μm in length, $50 - 30 \pm 5$ μm in width, and 2.7 ± 1 μm in thickness. These small resonators have been decorated by drop-casting robust core-shell $SCO@SiO_2$ NP systems with two different morphologies (87×54 nm and 87×28 nm). While the cores of these hybrid SCO NPs switches from the low-spin to the high-spin state, a systematic and reversible increase in the cantilever resonance frequency has been observed, consistently for various cantilever geometries and resonance modes. We have ascribed these hysteretic behaviours to variations of the surface stress (through the molecular volume change). Concomitantly with the abrupt resonant frequency upshift in the high-spin state a drop occurs in the quality factor and the reflected laser power. The former behaviour is related to the enhanced internal friction, most likely due to the increased contact areas of the NP/cantilever interfaces upon $LS \rightarrow HS$ state transition. The latter behaviour is rationalized through the cantilever bending as expected from the strong lattice expansion of the SCO NP upon the $LS \rightarrow HS$ state transition.

We have substantiated the experimental observations with numerical simulations providing a useful guideline for taking into account thermal effects, interfacial aspects, realistic cantilever geometry and SCO NP parameters. Associating MEMS/NEMS and cooperative SCO materials could thus bring new fundamental answers regarding the genuine role of struc-

tural/mechanical properties of SCO (nano)materials and open up new ways for smart sensing micro-nano devices retaining memory while operating at room temperature. Remarkably, this technique holds a high sensitivity already at the state-of-the-art for investigation of memory effects at the nanoscale comparable to the detection limit of a micro-magnetometer prototype reported recently as small as 2.10^{-6} mm^3 (in terms of particle volume).

Supporting Information

The Supporting Information is available free of charge on the ACS Publications website at DOI:.

> Schematic of optical lever system, TEM images of SCO NPs **1** and **2**, Table S1, Thermal variation of the magnetic susceptibility of **1** and **2**, Table S2-3, Details of COMSOL simulations, Table S4, Detailed analytical calculations and estimations, SEM image, Additional experimental data and numerical simulations.

Author information

Corresponding Author

*julien.dugay@gmail.com

*eugenio.coronado@uv.es

ORCID

Julien Dugay: 0000-0002-4384-1315

Eugenio Coronado: 0000-0002-1848-8791

Mónica Giménez-Marqués: 0000-0002-4931-5711

Nicola Manca: 0000-0002-7768-2500

References

(1) Newell, W. E. Miniaturization of Tuning Forks. *Science* **1968**, *161*, 1320–1326.

(2) Craighead, H. G. Nanoelectromechanical Systems. *Science* **2000**, *290*, 1532–1535.

(3) Binnig, G.; Quate, C. F.; Gerber, C. Atomic Force Microscope. *Physical Review Letters* **1986**, *56*, 930–933.

(4) Fritz, J.; Baller, M. K.; Lang, H. P.; Rothuizen, H.; Vettiger, P.; Meyer, E.; Güntherodt, H.-J.; Gerber, C.; Gimzewski, J. K. Translating Biomolecular Recognition into Nanomechanics. *Science* **2000**, *288*, 316–318.

(5) Lavrik, N. V.; Sepaniak, M. J.; Datskos, P. G. Cantilever transducers as a platform for chemical and biological sensors. *Review of Scientific Instruments* **2004**, *75*, 2229–2253.

(6) Singamaneni, S.; LeMieux, M. C.; Lang, H. P.; Gerber, C.; Lam, Y.; Zauscher, S.; Datskos, P. G.; Lavrik, N. V.; Jiang, H.; Naik, R. R.; Bunning, T. J.; Tsukruk, V. V. Bimaterial Microcantilevers as a Hybrid Sensing Platform. *Advanced Materials* **2008**, *20*, 653–680.

(7) Berger, R.; Delamarche, E.; Lang, H. P.; Gerber, C.; Gimzewski, J. K.; Meyer, E.; Güntherodt, H.-J. Surface Stress in the Self-Assembly of Alkanethiols on Gold. *Science* **1997**, *276*, 2021–2024.

(8) Rúa, A.; Cabrera, R.; Coy, H.; Merced, E.; Sepúlveda, N.; Fernández, F. E. Phase transition behavior in microcantilevers coated with M1-phase VO2 and M2-phase VO2:Cr thin films. *Journal of Applied Physics* **2012**, *111*, 104502.

(9) Manca, N.; Pellegrino, L.; Kanki, T.; Yamasaki, S.; Tanaka, H.; Siri, A. S.; Marré, D. Programmable Mechanical Resonances in MEMS by Localized Joule Heating of Phase Change Materials. *Advanced Materials* **2013**, *25*, 6430–6435.

(10) Gural'skiy, I. A.; Quintero, C. M.; Costa, J. S.; Demont, P.; Molnár, G.; Salmon, L.; Shepherd, H. J.; Bousseksou, A. Spin crossover composite materials for electrothermomechanical actuators. *Journal of Materials Chemistry C* **2014**, *2*, 2949–2955.

(11) Molnár, G.; Salmon, L.; Nicolazzi, W.; Terki, F.; Bousseksou, A. Emerging properties and applications of spin crossover nanomaterials. *Journal of Materials Chemistry C* **2014**, *2*, 1360–1366.

(12) Manrique-Juárez, M. D.; Mathieu, F.; Laborde, A.; Rat, S.; Shalabaeva, V.; Demont, P.; Thomas, O.; Salmon, L.; Leichle, T.; Nicu, L.; Molnár, G.; Bousseksou, A. Micromachining-Compatible, Facile Fabrication of Polymer Nanocomposite Spin Crossover Actuators. *Advanced Functional Materials* **2018**, *28*, 1801970.

(13) Mikolasek, M. et al. Complete Set of Elastic Moduli of a Spin-Crossover Solid: Spin-State Dependence and Mechanical Actuation. *Journal of the American Chemical Society* **2018**, *140*, 8970–8979.

(14) Manrique-Juarez, M. D.; Rat, S.; Mathieu, F.; Saya, D.; Séguy, I.; Leïchlé, T.; Nicu, L.; Salmon, L.; Molnár, G.; Bousseksou, A. Microelectromechanical systems integrating molecular spin crossover actuators. *Applied Physics Letters* **2016**, *109*, 061903.

(15) Cobo, S.; Ostrovskii, D.; Bonhommeau, S.; Vendier, L.; Molnár, G.; Salmon, L.; Tanaka, K.; Bousseksou, A. Single-Laser-Shot-Induced Complete Bidirectional Spin Transition at Room Temperature in Single Crystals of (FeII(pyrazine)(Pt(CN)4)). *Journal of the American Chemical Society* **2008**, *130*, 9019–9024.

(16) Gütlich, P.; Goodwin, H. A. *Spin crossover in transition metal compounds I*; Springer Verlag, 2004; Vol. 1.

(17) Manrique-Juárez, M. D.; Rat, S.; Salmon, L.; Molnár, G.; Quintero, C. M.; Nicu, L.; Shepherd, H. J.; Bousseksou, A. Switchable molecule-based materials for micro- and nanoscale actuating applications: Achievements and prospects. *Coordination Chemistry Reviews* **2016**, *308*, 395–408.

(18) Bousseksou, A.; Molnár, G.; Salmon, L.; Nicolazzi, W. Molecular spin crossover phenomenon: recent achievements and prospects. *Chemical Society Reviews* **2011**, *40*, 3313–3335.

(19) Prins, F.; Barreiro, A.; Ruitenberg, J. W.; Seldenthuis, J. S.; Aliaga-Alcalde, N.; Vandersypen, L. M. K.; van der Zant, H. S. J. Room-Temperature Gating of Molecular Junctions Using Few-Layer Graphene Nanogap Electrodes. *Nano Letters* **2011**, *11*, 4607–4611.

(20) Coronado, E.; Giménez-Marqués, M.; Mínguez Espallargas, G.; Rey, F.; Vitórica-Yrezábal, I. J. Spin-Crossover Modification through Selective CO2 Sorption. *Journal of the American Chemical Society* **2013**, *135*, 15986–15989.

(21) Cavallini, M. Status and perspectives in thin films and patterning of spin crossover compounds. *Physical Chemistry Chemical Physics* **2012**, *14*, 11867–11876.

(22) Dugay, J.; Giménez-Marqués, M.; Kozlova, T.; Zandbergen, H. W.; Coronado, E.; van der Zant, H. S. J. Spin Switching in Electronic Devices Based on 2D Assemblies of Spin-Crossover Nanoparticles. *Advanced Materials* **2015**, *27*, 1288–1293.

(23) Urdampilleta, M.; Ayela, C.; Ducrot, P.-H.; Rosario-Amorin, D.; Mondal, A.; Rouzières, M.; Dechambenoit, P.; Mathonière, C.; Mathieu, F.; Dufour, I.; Clérac, R. Molecule-based microelectromechanical sensors. *Scientific Reports* **2018**, *8*, 8016.

(24) Coronado, E.; Galán-Mascarós, J. R.; Monrabal-Capilla, M.; García-Martínez, J.; Pardo-Ibáñez, P. Bistable Spin-Crossover Nanoparticles Showing Magnetic Thermal Hysteresis near Room Temperature. *Advanced Materials* **2007**, *19*, 1359–1361.

(25) Galán-Mascarós, J. R.; Coronado, E.; Forment-Aliaga, A.; Monrabal-Capilla, M.; Pinilla-Cienfuegos, E.; Ceolin, M. Tuning Size and Thermal Hysteresis in Bistable Spin Crossover Nanoparticles. *Inorganic Chemistry* **2010**, *49*, 5706–5714.

(26) Giménez-Marqués, M.; Larrea, M. L. G.-S. d.; Coronado, E. Unravelling the chemical design of spin-crossover nanoparticles based on iron(ii)–triazole coordination polymers: towards a control of the spin transition. *Journal of Materials Chemistry C* **2015**, *3*, 7946–7953.

(27) Torres-Cavanillas, L., R.and Lima-Moya; Tichelaar, F. D.; Zandbergen, H.; Giménez-Marqués, M.; Coronado, E. Limiting the size of hybrid Fe-triazole@SiO2 spin-crossover nanoparticles. **Submitted 2018**,

(28) Blom, F. R.; Bouwstra, S.; Elwenspoek, M.; Fluitman, J. H. J. Dependence of the quality factor of micromachined silicon beam resonators on pressure and geometry. *Journal of Vacuum Science & Technology B: Microelectronics and Nanometer Structures Processing, Measurement, and Phenomena* **1992**, *10*, 19–26.

(29) Titos-Padilla, S.; Herrera, J. M.; Chen, X.-W.; Delgado, J. J.; Colacio, E. Bifunctional Hybrid SiO2 Nanoparticles Showing Synergy between Core Spin Crossover and Shell Luminescence Properties. *Angewandte Chemie* **2011**, *123*, 3348–3351.

(30) Raza, Y.; Volatron, F.; Moldovan, S.; Ersen, O.; Huc, V.; Martini, C.; Brisset, F.; Gloter, A.; Stéphan, O.; Bousseksou, A.; Catala, L.; Mallah, T. Matrix-dependent cooperativity in spin crossover Fe(pyrazine)Pt(CN)4 nanoparticles. *Chemical Communications* **2011**, *47*, 11501–11503.

(31) Mahmoud, M. A. Validity and Accuracy of Resonance Shift Prediction Formulas for Microcantilevers: A Review and Comparative Study. *Critical Reviews in Solid State and Materials Sciences* **2016**, *41*, 386–429.

(32) Holovchenko, A.; Dugay, J.; Giménez-Marqués, M.; Torres-Cavanillas, R.; Coronado, E.; van der Zant, H. S. J. Near Room-Temperature Memory Devices Based on Hybrid Spin-Crossover@SiO2 Nanoparticles Coupled to Single-Layer Graphene Nanoelectrodes. *Advanced Materials* **2016**, *28*, 7228–7233.

(33) Karabalin, R. B.; Villanueva, L. G.; Matheny, M. H.; Sader, J. E.; Roukes, M. L. Stress-Induced Variations in the Stiffness of Micro- and Nanocantilever Beams. *Physical Review Letters* **2012**, *108*, 236101.

(34) Tanasa, R.; Stancu, A.; Létard, J.-F.; Codjovi, E.; Linares, J.; Varret, F. Piezo- and thermo-switch investigation of the spin-crossover compound [Fe(PM-BiA)2(NCS)2]. *Chemical Physics Letters* **2007**, *443*, 435–438.

(35) Linares, J.; Codjovi, E.; Garcia, Y. Pressure and Temperature Spin Crossover Sensors with Optical Detection. *Sensors* **2012**, *12*, 4479–4492.

(36) Diaconu, A.; Lupu, S.-L.; Rusu, I.; Risca, I.-M.; Salmon, L.; Molnár, G.; Bousseksou, A.; Demont, P.; Rotaru, A. Piezoresistive Effect in the [Fe(Htrz)2(trz)](BF4) Spin Crossover Complex. *The Journal of Physical Chemistry Letters* **2017**,

(37) Slimani, A.; Khemakhem, H.; Boukheddaden, K. Structural synergy in a core-shell spin crossover nanoparticle investigated by an electroelastic model. *Physical Review B* **2017**, *95*, 174104.

(38) Félix, G.; Mikolasek, M.; Molnar, G.; Nicolazzi, W.; Bousseksou, A. Control of the phase stability in spin crossover core-shell nanoparticles through elastic interface energy. *European Journal of Inorganic Chemistry* **2017**, n/a–n/a.

(39) Mikolasek, M.; Félix, G.; Peng, H.; Rat, S.; Terki, F.; Chumakov, A. I.; Salmon, L.; Molnár, G.; Nicolazzi, W.; Bousseksou, A. Finite-size effects on the lattice dynamics in spin crossover nanomaterials. I. Nuclear inelastic scattering investigation. *Physical Review B* **2017**, *96*, 035426.

(40) Venstra, W. J.; Capener, M. J.; Elliott, S. R. Nanomechanical gas sensing with nonlinear resonant cantilevers. *Nanotechnology* **2014**, *25*, 425501.

(41) Lefter, C.; Tan, R.; Dugay, J.; Tricard, S.; Molnár, G.; Salmon, L.; Carrey, J.; Rotaru, A.; Bousseksou, A. Light induced modulation of charge transport phenomena across the bistability region in [Fe(Htrz)2(trz)](BF4) spin crossover micro-rods. *Physical Chemistry Chemical Physics* **2015**, *17*, 5151–5154.

(42) Shepherd, H. J.; Gural'skiy, I. A.; Quintero, C. M.; Tricard, S.; Salmon, L.; Molnár, G.; Bousseksou, A. Molecular actuators driven by cooperative spin-state switching. *Nature Communications* **2013**, *4*.

(43) Privorotskaya, N. L.; King, W. P. Silicon microcantilever hotplates with high temperature uniformity. *Sensors and Actuators A: Physical* **2009**, *152*, 160–167.

(44) Manrique-Juarez, M. D.; Mathieu, F.; Shalabaeva, V.; Cacheux, J.; Rat, S.; Nicu, L.; Leïchlé, T.; Salmon, L.; Molnár, G.; Bousseksou, A. A Bistable Microelectromechanical System Actuated by Spin-Crossover Molecules. *Angewandte Chemie* **2017**, *129*, 8186–8190.

(45) Urdampilleta, M.; Ducrot, P.-H.; Rosario-Amorin, D.; Mondal, A.; Rouzières, M.; Dechambenoit, P.; Mathonière, C.; Mathieu, F.; Dufour, I.; Ayela, C.; Clérac, R. Molecule-based microelectromechanical sensors. *arXiv:1701.01341 [cond-mat]* **2017**, arXiv: 1701.01341.

(46) Hernández, E. M.; Quintero, C. M.; Kraieva, O.; Thibault, C.; Bergaud, C.; Salmon, L.; Molnár, G.; Bousseksou, A. AFM Imaging of Molecular Spin-State Changes through Quantitative Thermomechanical Measurements. *Advanced Materials* **2014**, *26*, 2889–2893.

(47) Urakawa, A.; Van Beek, W.; Monrabal-Capilla, M.; Galán-Mascarós, J. R.; Palin, L.; Milanesio, M. Combined, Modulation Enhanced X-ray Powder Diffraction and Raman Spectroscopic Study of Structural Transitions in the Spin Crossover Material [Fe(Htrz)2(trz)](BF4)†. *The Journal of Physical Chemistry C* **2011**, *115*, 1323–1329.